Ultraviolet resonance Raman study of the pyrene S_4, S_3, and S_2 excited electronic states

Colleen M. Jones and Sanford A. Asher[a)]
Department of Chemistry, University of Pittsburgh, Pittsburgh, Pennsylvania 15260

(Received 23 February 1988; accepted 26 May 1988)

UV resonance Raman excitation within the S_2, S_3, and S_4 $\pi \rightarrow \pi^*$ electronic transitions of pyrene results in strong enhancement of totally symmetric ring vibrations. The Raman modes most strongly enhanced within these electronic transitions derive from vibrations exhibiting Franck–Condon vibronic structure in the absorption spectrum. The 1597 cm^{-1} (b_{3g}) mode shows selective enhancement between the S_3 and S_4 transitions, and between the S_2 and S_3 transitions due to Herzberg–Teller coupling between these symmetry-allowed states. The experimentally observed S_4 resonance Raman excitation profiles of the totally symmetric pyrene fundamentals agree closely with those calculated using resonance Raman transform theory if non-Condon contributions are included. We see an increased non-Condon contribution with an increasing vibrational frequency, indicating nonadiabatic vibronic interactions. The high incident energy fluxes of the Nd-YAG laser-based excitation source cause saturation of the pyrene Raman intensities since molecular absorption depletes the ground state population. The long-lived S_1 singlet excited state bottlenecks relaxation back to the ground electronic state. Formation of pyrene phototransients is also observed with high incident energy fluxes at particular excitation wavelengths.

INTRODUCTION

Recently there has been great interest in the use of theoretical methods to predict Raman excitation profile (RREP) band shapes in order to derive information on excited state potential energy surfaces.[1–8] Major interest has centered on use of the recently developed resonance Raman transform theory to relate the RREP to the observed absorption spectrum. The transform theory relies on the multimode information contained in the absorption spectrum to link, via the optical theorem, absorption to Raman scattering. Quantitative excited state parameters can be obtained by fitting observed Raman cross section excitation profiles to the theoretically predicted excitation profiles. This approach has successfully predicted the resonance Raman excitation profiles of totally symmetric Raman-active vibrational modes of biologically important molecules such as β-carotene, the Soret-enhanced porphyrin vibrations of the heme protein cytochrome *c*, and the ring vibrations enhanced within the S_1 electronic transition of the polycyclic aromatic hydrocarbon, azulene.[1(a)–1(c),6,8] These excitation profile studies were used to test the applicability of transform theory, to study excited molecular electronic states, and to refine and extend the transform formalism.

We report here a comprehensive UV Raman excitation profile investigation of the S_2, S_3, and S_4 $\pi \rightarrow \pi^*$ electronic transitions of pyrene. The objectives of this study are to increase the understanding of the optical transitions of this large polycyclic aromatic hydrocarbon, to examine the coupling of resonantly enhanced vibrational modes to pyrene's various excited states, and to provide a further experimental test of the transform theory formalism. These intense pyrene electronic transitions should uniquely fulfill the basic assumptions of the transform theory. The S_2, S_3, and S_4 electronic transitions show strong Franck–Condon structure, indicating that the Raman intensities of the totally symmetric Raman-active modes derive from Raman *A*-term scattering. Further, the spacing between the transitions is large compared to their bandwidths.

The recent development of UV Raman instrumentation now permits investigation of higher excited states of aromatic molecules. Despite the wealth of information that exists on the electronic and vibrational structure of polycyclic aromatic hydrocarbons (PAH), little detailed experimental information exists for transitions above the first singlet and triplet states. We have already reported on UV resonance Raman spectroscopic studies of various PAHs in complex matrices such as coal liquids and rat liver microsomes with excitation into high-lying PAH excited electronic states.[9–11] Generally, PAH $\pi \rightarrow \pi^*$ transitions above S_1 show high oscillator strengths, and large resonance Raman enhancements occur for those totally symmetric vibrational modes coupled to these strong dipole-allowed transitions. Raman excitation profiles, which monitor the frequency dependence of the cross sections of Raman-active vibrational modes, provides information on the ground state and excited state geometry as well as information on the coupling of vibrations to the resonant excited electronic potential energy surface.[12]

As part of this RREP study we also characterized various pyrene photophysical processes which occur with UV excitation. This follows our recent studies of the effects of high incident pulsed energy fluxes upon Raman saturation, and upon the formation of photochemical and excited state intermediates for tyrosinate and pyrene with excitation within their $S_2(L_a)$ and $S_4(B_{1u})\pi \rightarrow \pi^*$ transitions, respectively.[13] We demonstrate here methods for correcting the

[a)] Corresponding author.

 0021-9606/88/172649-13$02.10 © 1988 American Institute of Physics

Downloaded 22 Jan 2009 to 130.49.228.46. Redistribution subject to AIP license or copyright; see http://jcp.aip.org/jcp/copyright.jsp

measured Raman intensities for saturation in order to quantitatively determine excitation profile Raman cross sections. We compare the experimental Raman excitation profiles to excitation profiles calculated using transform theory.

EXPERIMENTAL

Solutions of pyrene, (Chem Service Inc., West Chester, PA; 99%$^+$ purity) at concentrations of 10^{-3}–10^{-4} M were dissolved in spectral grade acetonitrile (Burdick and Jackson) and were recirculated through a Suprasil quartz capillary (1.0 mm inner diameter). The frequency doubled output of a Q-switched Quanta-Ray DCR-2A Nd-YAG laser operated at 20 Hz was used to pump a dye laser. The dye laser output was either frequency doubled or doubled and mixed with the 1064 nm YAG fundamental to obtain the 220–340 nm excitations (6 ns pulse widths) used in this study. A 90° scattering geometry was employed and Raman scattered light was imaged onto the slit of a modified Spex Triplemate monochromator by an ellipsoidal mirror. A crystalline quartz polarizing wedge was used to eliminate the polarization bias of the monochromator. The 1200 groove/mm grating used in the spectrograph stage of the Triplemate gave a spectral resolution ~ 12 cm^{-1} at 240 nm and ~ 8 cm^{-1} at 300 nm. The Raman scattered light was detected by using an EG&G PAR model 1420 blue-intensified Reticon detector interfaced to a PAR OMA II console. This UV Raman spectrometer is described in detail elsewhere.[14] Typical accumulation times were 15 min or less. For the excitation profile data, laser energy fluxes at the sample were maintained below levels where photochemistry or phototransient formation occurs by using soft focusing (estimated beam diameter $\geqslant 500$ μm at the sample) and low incident laser pulse energies (< 0.15 mJ/pulse).

The "unsaturated" pyrene cross sections were obtained by utilizing the procedure demonstrated earlier which monitors the dependence upon the incident laser energy flux of the relative intensities of the analyte bands to the internal standard band.[13,15,16] In the absence of saturation the Raman intensities depend linearly on the incident energy flux. In contrast, molecules excited in resonance will absorb light and undergo transitions into excited states which will depopulate the ground state. The magnitude of depopulation can be high with the high energy flux conditions associated with pulsed laser sources; the Raman intensities under such conditions will show sublinear dependences upon the excitation intensity.

The saturated pyrene Raman intensities, I_p (photons/s sr) at relatively low laser fluxes will exhibit a linear dependence on the incident energy flux, I_0 (photons/s cm^2):

$$I_p = \sigma_p I_0 N_p [1 - \sigma_A I_0/2], \tag{1}$$

where σ_p is the differential Raman cross section of the pyrene vibrational band (cm^2/molecule sr), N_p is the number of pyrene molecules in the illuminated sample volume, and σ_A is the molar absorptivity at the incident laser frequency.

The non-absorbing internal standard scattering intensity I_s remains directly proportional to the incident energy flux:

$$I_s = \sigma_s I_0 N_s, \tag{1a}$$

where σ_s is the Raman scattering cross section of the internal standard and N_s is the number of molecules of the internal standard in the sampling volume.

Thus, the relative intensity ratio of the pyrene to the acetonitrile internal standard band R can be written as

$$R = \frac{\sigma_p C_p}{\sigma_s C_s}\left[1 - \frac{\sigma_A I_0}{2}\right], \tag{2}$$

where C_p and C_s (the concentration of pyrene and the internal standard, respectively) have been substituted for N_p and N_s since the number of molecules is directly proportional to their concentrations. At low incident energy fluxes, the relative intensity ratio decreases linearly as the excitation flux increases. The intercept of a plot of the relative intensity ratio vs the incident energy flux is proportional to the ratio of the Raman cross sections of the analyte to the internal standard bands. The intensities of the pyrene bands relative to one another *within* a spectrum are, of course, independent of the excitation energy flux even at fluxes where Raman saturation occurs; saturation effects only the total number of ground state analyte molecules available for Raman scattering.

This model is applied for the first time to obtain excitation profile data for pyrene, a molecule whose unsaturated excitation profiles cannot be measured with adequate signal-to-noise at 240 nm with our 20 Hz YAG laser excitation source. We confirmed the reliability of our extrapolation technique for pyrene by comparing extrapolated Raman cross sections to those obtained using a longer pulse width (16 ns), higher repetition rate 200 Hz excimer laser that delivers a tenfold smaller pulse energy.[13]

We expect that the maximum likely relative error (± 2 standard deviations) in the RREP cross section measurements is less than 25%. The extrapolated relative intensities were corrected for monochromator efficiency and were converted to total differential Raman cross sections using the method of Dudik *et al.*[17] The total differential Raman cross section of the 918 cm^{-1} acetonitrile band, which was previously shown to increase almost as ν_0^4, was used as the internal standard. The intensities of the 1408 and 1553 cm^{-1} pyrene modes were obtained from difference spectra where the overlapping contributions of the 1376 and 1440 cm^{-1} acetonitrile bands were numerically removed.

Self-absorption was found to negligibly affect the excitation profile data due to the small "effective" absorption path lengths which appear to be less than 100 μm. We experimentally verified this by comparing the relative intensities of the CH_3CN solvent bands at 918 and 1376 cm^{-1} in both pure solution and in our pyrene sample solutions. The effective sample self-absorption path length changes as a function of excitation wavelength and sample optical positioning. From our experimental study of self-absorption we conclude that the maximum self-absorption induced systematic deviation is less than 15%.

RESULTS

Figure 1 shows the solution absorption spectrum of pyrene's electronic transitions to the S_4, S_3, and S_2 singlet states at 240 (B_{1u}), 272 (B_{2u}), and 334 (B_{1u}) nm, respective-

Downloaded 22 Jan 2009 to 130.49.228.46. Redistribution subject to AIP license or copyright; see http://jcp.aip.org/jcp/copyright.jsp

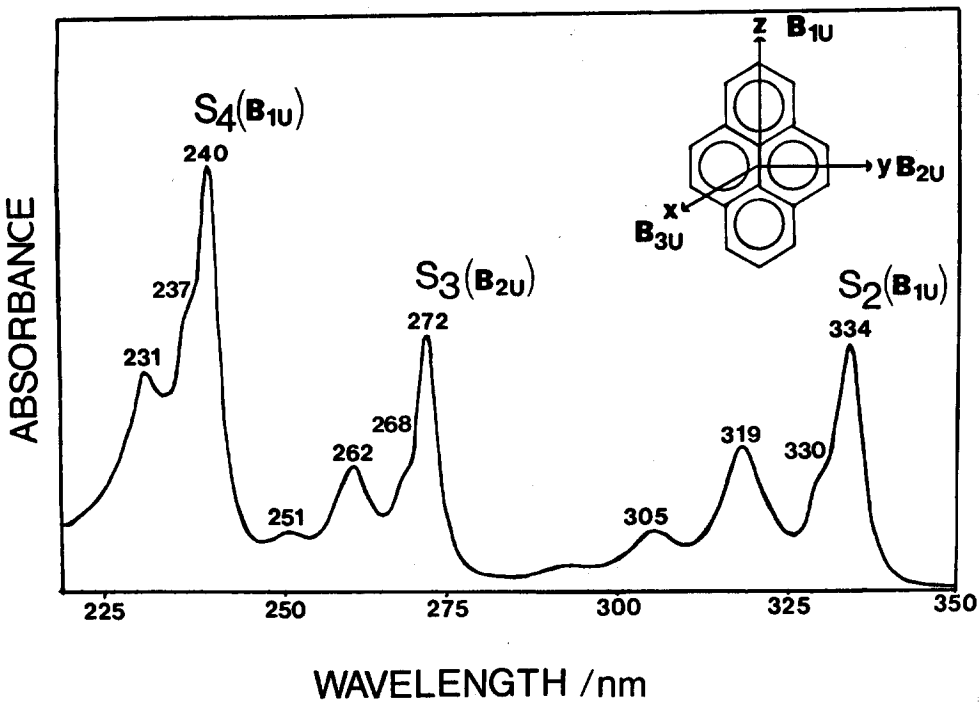

FIG. 1. UV absorption spectrum of pyrene in acetonitrile. Electronic symmetry assignments use the Mulliken convention (Ref. 18).

ly.[18,19] These strong dipole-allowed $\pi \rightarrow \pi^*$ electronic transitions are alternately polarized along the long and short pyrene molecular axes as indicated in Fig. 1. The weak absorption band due to the $S_1(B_{2u})$ electronic transition at 371 nm is not shown. This B_{2u} symmetry-allowed but orbitally forbidden transition shows a low oscillator strength, with its intensity deriving mainly from vibronic coupling mechanisms.[20] The S_4, S_3, and S_2 pyrene singlet electronic transitions exhibit strong 0–0 absorption maxima and complex Franck–Condon vibronic progressions.

Typical resonance Raman spectra of pyrene obtained at excitation within the S_4, S_3, and S_2 electronic states are shown in Figs. 2(a)–2(c), respectively. Raman excitation was restricted to the S_4–S_2 electronic bands since fluorescence interference overwhelms the Raman intensities within the S_1 transition. The pyrene Raman intensities can vary nonlinearly with the incident laser power due to optical saturation (*vide supra*). In addition, phototransient Raman bands can be induced with sufficiently high laser intensities for particular excitation wavelengths. The spectra displayed in Figs. 2(a)–2(c), and those used to obtain excitation profile data, were acquired using excitation powers below that where phototransient formation and permanent sample photochemistry was observed. The Raman bands at 380, 918, 1376, and 1440 cm^{-1} (shoulder) which derive from the solvent, acetonitrile, are shaded in Figs. 2(a)–2(c). The enhanced pyrene ring fundamental vibrations appear between 400 and 1650 cm^{-1} and exhibit a strong excitation wavelength dependence throughout the three $\pi \rightarrow \pi^*$ electronic transitions. Table I lists the pyrene fundamental vibrations observed in our study and in the earlier normal Raman study by Bree *et al.* along with their symmetry assignments which derived from depolarization ratio measurements.[21] Also included in Table I are Mecke and Klee's vibrational assignments.[22] Obviously, the totally symmetric pyrene ring vibrations are most strongly resonantly enhanced throughout these three electronic transitions. The 1597 cm^{-1} (b_{3g}) mode is the only nontotally symmetric mode significantly enhanced.

Figure 2(a) shows resonance Raman spectra of pyrene excited within its S_4 electronic transition. The vibrations most strongly enhanced by this electronic transition appear at 592, 1067, 1179, 1408, 1553, and 1632 cm^{-1}. The 592 and 1632 cm^{-1} modes and their overtones and combinations dominate the S_4 resonance Raman spectra. The first overtone of the 592 cm^{-1} mode occurs at 1184 cm^{-1} and most likely contributes to the intensity of the observed 1179 cm^{-1} band. Bree *et al.* tentatively assigned a 1174 cm^{-1} mode to a nontotally symmetric b_{3g} fundamental based on depolarization data from a normal Raman study, while Mecke and Klee assign an 1184 cm^{-1} mode to a totally symmetric pyrene fundamental.[21,22] The depolarization ratio of the 1179 cm^{-1} mode measured within S_4 indicates that it is totally symmetric and must therefore derive from the vibration assigned by Mecke and Klee. The 1179 cm^{-1} band intensity most likely derives from contributions from both the 1184 cm^{-1} fundamental and from the first overtone of the 592 cm^{-1} mode. The 1770 cm^{-1} vibration enhanced at 225 nm is possibly the second overtone of the 592 cm^{-1} mode.

Strong overtone and combination band activity was observed in the resonance Raman spectra at 228 nm which corresponds to excitation within the 231 nm S_4 absorption feature. Figure 3 shows the high frequency Raman spectral region above 1600 cm^{-1} for excitation within each of the $\pi \rightarrow \pi^*$ electronic transitions. Tentative assignments for the intense bands are included in each spectrum; due to the nu-

Downloaded 22 Jan 2009 to 130.49.228.46. Redistribution subject to AIP license or copyright; see http://jcp.aip.org/jcp/copyright.jsp

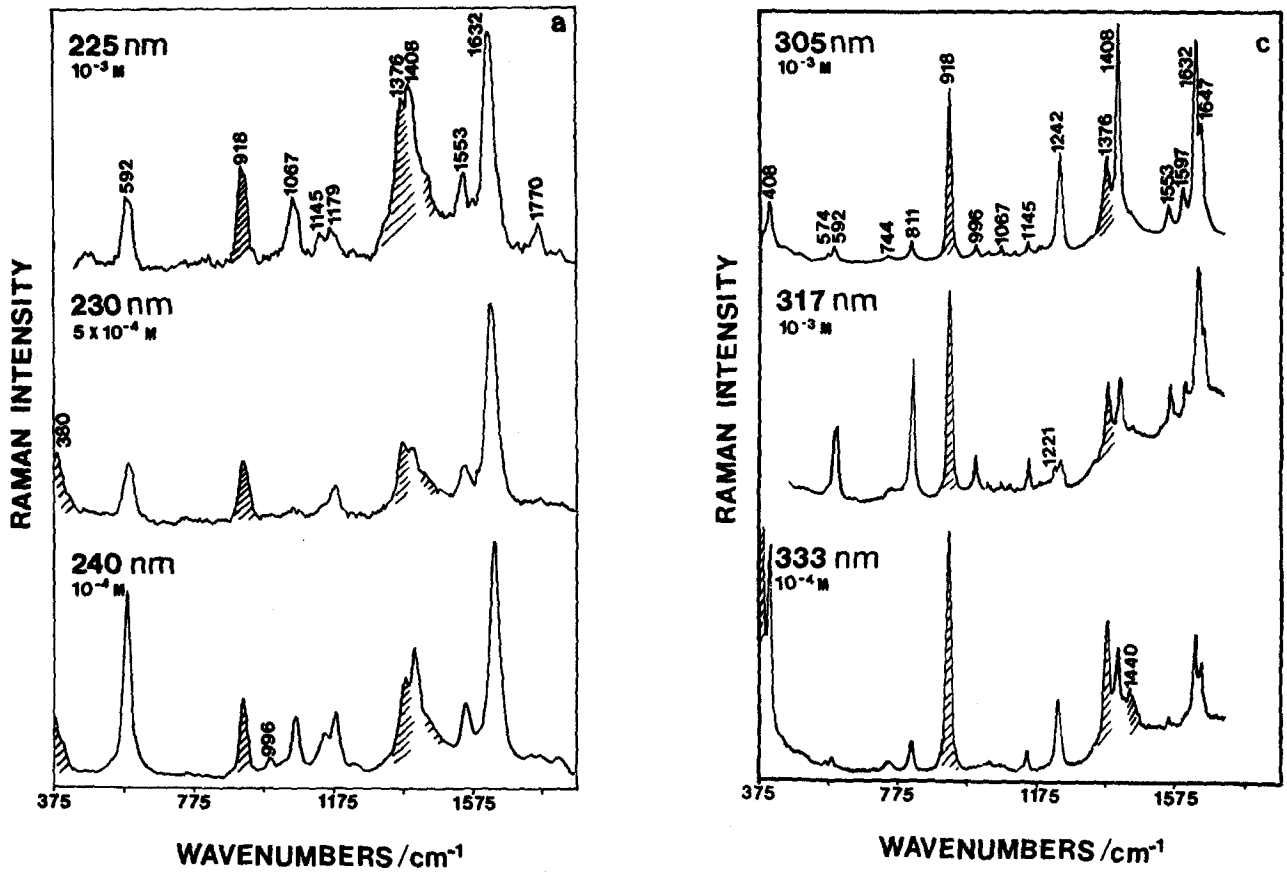

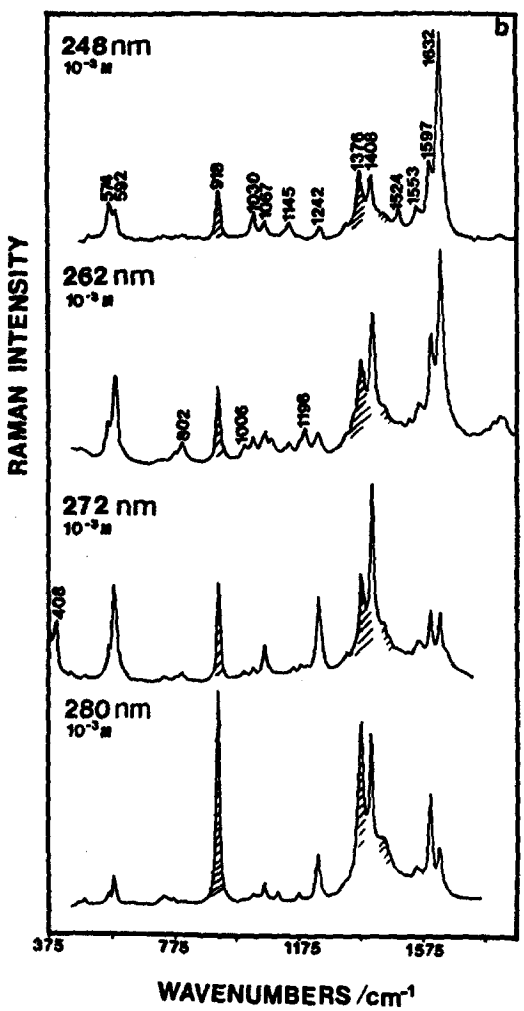

FIG. 2. UV resonance Raman spectra of pyrene in acetonitrile at various excitation wavelengths throughout the S_4 (a), S_3 (b), and S_2 (c) electronic transitions. Solvent bands are shaded in the figure and sample concentrations vary as indicated. Pyrene Raman intensities show saturation and are artifactually decreased relative to that of the acetonitrile bands.

Downloaded 22 Jan 2009 to 130.49.228.46. Redistribution subject to AIP license or copyright; see http://jcp.aip.org/jcp/copyright.jsp

TABLE I. Pyrene fundamental frequencies and vibrational assignments.

Frequency (cm^{-1})	Symmetry[a]	Vibrational type[b]
221	B_{2g}	
256	B_{1g}	
408	A_g	ω[d]
458	B_{3g}?[c]	
505	B_{3g}	
592	A_g	ω
737	B_{3g}	
773	B_{2g}	
802	A_g	
844	B_{2g} or B_{3g}	
904	?	
958	B_{3g} or B_{2g}	
970	B_{2g} ?	
1006	A_g	
1040	A_g	
1067	A_g	δ?[c]
1110	B_{3g}	
1145	A_g	δ
1174	B_{3g}?	ω?
1192	A_g	
1199	A_g	
1212	A_g	
1233	A_g	
1242	A_g	
1327	A_g	
1351	A_g	
1358	A_g	
1370	B_{3g}	
1395	A_g	
1408	A_g	ω
1426	A_g	ω
1462	A_g	
1504	A_g	
1553	A_g	
1562	A_g	
1597	B_{3g}	ω
1632	A_g	ω
1647	A_g	
1665	A_g	
1697	A	
3024	A_g	
3059	A_g	
3103	A_g	

[a] See Ref. 21. Assignments made using the Mulliken convention (Ref. 18).
[b] See Ref. 22.
[c] ?—tentative assignment.
[d] ω—vibration involving motion of the carbon atoms in the molecular plane.
[e] δ—vibration involving a change in the angle between two neighboring carbon atoms and a hydrogen atom bonded to one of the carbons.

merous pyrene fundamental vibrations, some alternative assignments are also possible. As can be seen from the spectrum excited at 228 nm, combinations and overtones of the 592 and 1632 cm^{-1} modes dominate the high frequency Raman spectral region for excitation in S_4. The overtone and combination intensities are comparable to those of the fundamentals. Direct correspondences between the S_4 absorption spectral features (Fig. 1) and the strongest enhanced Raman modes are evident. The shoulder that appears $\sim$550 cm^{-1} (237 nm) to higher energy from the 240 nm absorption band maximum, and the 231 nm vibronic feature [$\sim$1600 cm^{-1} (231 nm) from the absorption maximum] reflect strong Franck–Condon activity of the 592 and 1632 cm^{-1} pyrene fundamentals, respectively.

Figure 2(b) shows the resonance Raman spectra obtained at excitation within the S_3 electronic transition. Vibronic progressions are observed in the absorption spectrum at $\sim$500 and 1400 cm^{-1} from the 272 nm electronic absorption band maximum. The prominent Raman bands occur at 408, 592, 1242, 1408, and 1632 cm^{-1}. New low frequency Raman bands at 408 cm^{-1} (totally symmetric) and 574 cm^{-1} appear that are not observed for excitation within S_4. The 574 cm^{-1} mode is not observed in the normal Raman spectra of pyrene, and may derive from a vibration enhanced uniquely in S_3. The 408 and 592 cm^{-1} pyrene fundamentals contribute to the intensity of the $\sim$268 nm shoulder of the S_3 absorption maximum, while the 1408 cm^{-1} mode is the primary contributor to the Franck–Condon vibronic absorption feature at 262 nm. The 1632 cm^{-1} mode exhibits an unusual behavior for excitation in S_3. The intensity of this totally symmetric mode is at a minimum at the 272 nm S_3 absorption maximum. The 1632 cm^{-1} band intensity, however, becomes strong again in resonance with the S_2 transition.

Complex overtone and combination spectra are obtained with excitation at 261 nm which is within the 262 nm S_3 absorption feature (see Fig. 3). Many weak bands appear in the high frequency region. Several of the strong bands are clearly assignable to combinations or overtones involving the 1408 cm^{-1} mode; the 1408 cm^{-1} mode dominates the resonance Raman spectrum obtained with excitation within the S_3 electronic absorption band maximum.

A 1597 cm^{-1} band with a depolarization ratio of 1.2 (263 nm excitation) is observed with moderate intensity with excitation in S_3 [see Fig. 2(b)]. This inversely polarized b_{3g} vibration is the only nontotally symmetric mode which appears with moderate intensity; other b_{3g} modes are only very weakly enhanced. All of the other vibrations were polarized. Table II lists measured depolarization ratios for prominent pyrene vibrations with excitation in the S_4, S_3, and S_2 electronic transitions. A depolarization ratio of 0.33 will occur if one diagonal element of the polarizability tensor dominates; this occurs, for example, for a transition polarized along a single coordinate axis. Table II shows that many of the depolarization ratios are close to 0.33, as would be expected for excitation in these linearly polarized transitions. Any small deviation from 0.33 in the measured depolarization ratios could derive from preresonance contributions from adjacent, alternately polarized electronic transitions or from experimental error. Large deviations must signal the presence of overlapping vibrations or the mixing in of a perpendicularly polarized electronic transition.

The resonance Raman spectra of pyrene excited within the S_2 electronic transition are shown in Fig. 2(c). Fluorescence from the S_1 state begins to interfere towards longer wavelength. The S_2 absorption band exhibits Franck–Condon vibronic features $\sim$400 cm^{-1} (330 nm), 1400 cm^{-1}

Downloaded 22 Jan 2009 to 130.49.228.46. Redistribution subject to AIP license or copyright; see http://jcp.aip.org/jcp/copyright.jsp

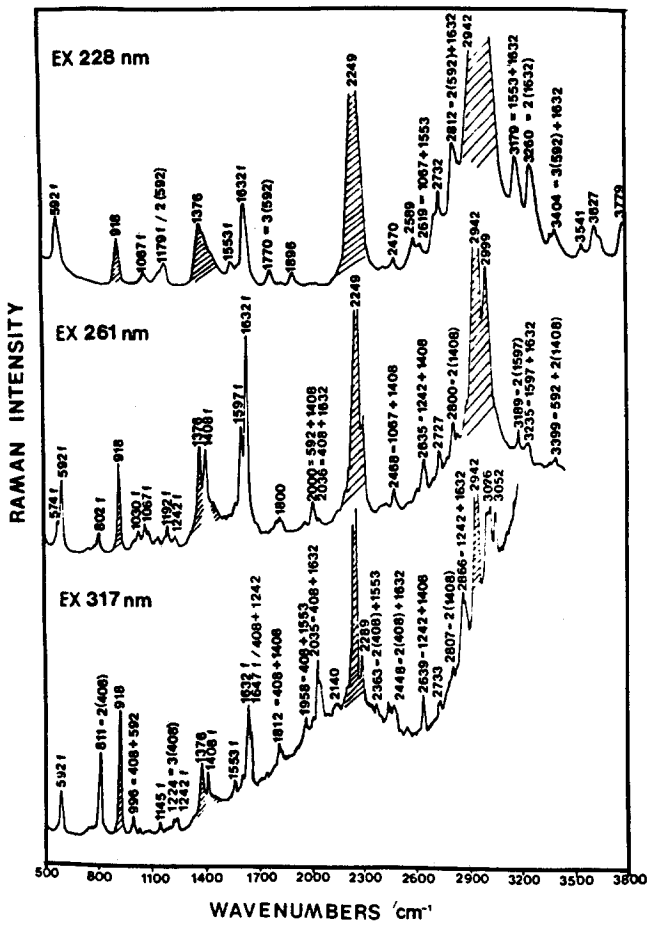

FIG. 3. UV resonance Raman spectra of the pyrene fundamentals (f) and of the combinations and overtones observed with 228, 261, and 317 nm excitation. Solvent bands are shaded, and tentative overtone and combination vibrational assignments for the high frequency Raman modes are included in the figure.

(319 nm), and 2850 cm^{-1} (305 nm) on the high energy side of the 334 nm band maximum. Vapor phase absorption studies of pyrene clearly resolve the 400 cm^{-1} S_2 vibronic feature from the 0–0 transition as a 408 cm^{-1} pyrene vibration.[23] In contrast, the high energy shoulder of the 272 nm S_3 maximum evident in the solution absorption spectrum is not resolvable in the vapor phase, presumably due to overlapping contributions of other low frequency vibrations, or because of the large linewidths of the underlying transitions.

The Raman vibrational modes most strongly enhanced with S_2 resonant excitations occur at 408, 1242, 1408, and 1632 cm^{-1}. The 1647 cm^{-1} Raman band, which appears in S_2 and is enhanced throughout the transition, probably corresponds to the 1647 cm^{-1} totally symmetric fundamental vibration observed by Bree *et al.* in their normal Raman study of pyrene.[21] Overtones and combinations involving the low frequency 408 cm^{-1} mode are readily observed at 317 nm excitation within the 319 nm S_2 absorption feature (see Fig. 3). The observed band at 811 cm^{-1} contains contributions from the overtone of the 408 cm^{-1} mode and from a pyrene fundamental at this frequency. The 1221 cm^{-1} band, resonantly enhanced within S_2, derives from the second overtone of the 408 cm^{-1} mode; no fundamental occurs at this frequency. Tentative overtone and combination band assignments for the higher frequency Raman modes observed at 317 nm are shown in Fig. 3. These assignments parallel those of a low temperature fluorescence study of pyrene where fluorescent emission from S_1 also showed strong activity of the 408 and 1408 cm^{-1} modes as overtones and combinations.[24] Different overtone and combination bands are, as expected, observed in the Raman spectra excited within the S_4, S_3, and S_2 electronic transitions. The new Raman bands at 3026 and 3052 cm^{-1} with 317 nm excitation are likely to derive from overtone and combination bands since we expect little enhancement of C–H stretching by these $\pi \rightarrow \pi^*$ transitions.

The Raman intensities observed are strongly influenced by saturation phenomena. The resonance Raman spectra shown in Fig. 2 show decreased pyrene intensities relative to the acetonitrile solvent bands compared to that obtained from unsaturated resonance Raman spectra. As discussed in the experimental section we determined the Raman cross sections for the excitation profile data by extrapolating the Raman intensities to zero incident energy flux.

Figure 4 shows the experimental resonance Raman excitation profiles (RREPs) of the totally symmetric 592, 1067, 1408, 1553, and 1632 cm^{-1} vibrations throughout the S_4 absorption band (filled circles); the solution absorption spectrum is also shown for comparison in the upper left-hand panel. The RREP of the 1179 cm^{-1} mode was not plotted since its intensity derives from overlapping contributions of a fundamental and the overtone of the 592 cm^{-1} mode. The solid curves in Fig. 4 show RREPs calculated using the basic Condon resonance Raman transform theory (*vide infra*). In addition, the broken curves show RREPs calculated by transform theory which includes linear non-Condon coupling. The RREP calculated using the transform theory restricted to the Condon approximation deviate significantly from measured excitation profiles. Only the 592 cm^{-1} RREP shows even qualitative agreement. The deviation between theory and experiment increases as the vibrational frequency of the band increases.

The RREP calculated from transform theory that includes non-Condon contributions accurately model the experimental RREP. Deviations of the data from the predicted RREP for the 1553 and 1632 cm^{-1} modes are well within experimental error. The larger differences observed for the 1408 cm^{-1} mode are associated with an increased experimental error for this band, since it strongly overlaps the 1376 and 1440 cm^{-1} acetonitrile solvent bands and its intensity must be determined by difference spectral measurements. The maximum resonance Raman cross section of the 592 cm^{-1} mode, the mode most strongly coupled to the S_4 electronic transition, is 64 b/sr (1 b = 10^{-24} cm^2/molecules) with 240 nm excitation. The 1632 cm^{-1} mode is also strongly coupled to S_4 and shows a maximum cross section of 54 b/sr at 240 nm.

Downloaded 22 Jan 2009 to 130.49.228.46. Redistribution subject to AIP license or copyright; see http://jcp.aip.org/jcp/copyright.jsp

TABLE II. Depolarization ratios of the intense pyrene fundamental vibrations.

Excitation wavelength	Depolarization ratios[d]				
	592	1408	1553	1597	1632 cm^{-1}
Ex = 243 nm[d]	0.33	b	0.44	a	0.36
Ex = 263 nm	0.34	0.53	0.73	1.2	0.41
Ex = 317 nm	0.40	0.37	0.36	0.31[e]	0.37
Normal Raman[c]	0.05	0.14	0.08	0.70	0.12

[a] Peak is absent at this wavelength.
[b] Peak intensity is small and overlaps significantly with other Raman bands.
[c] See Ref. 21. Excitation wavelength is 632.8 nm.
[d] Estimated error in the depolarization ratio measurements is less than 10% ($\pm 2\sigma$) for the strong bands and as much as 20% ($\pm 2\sigma$) for the weaker bands.
[e] The vibration observed at 1597 cm^{-1} at 317 nm may derive from a combination or overtone rather than from the 1597 cm^{-1} b_{3g} fundamental.

The high energy flux of the Nd-YAG laser excitation pulse induces saturation of the Raman intensities. Saturation is most apparent for excitation at wavelengths of high molar absorptivity. We have recently characterized the saturation that results with UV pulsed excitation for phenol and the aromatic amino acids trytophan and tyrosine.[15,16] Figure 5 shows the UVRR spectra of pyrene excited at 311 nm with incident energy fluxes of ~250(A) and 2.5(B) mJ/cm^2 pulse along with the difference spectrum (C). The pyrene intensities relative to the internal standard obviously strongly depend upon incident energy flux, while the intensities of the pyrene peaks relative to one another are independent of laser energy. In addition to saturation, phototransient formation is evident in the higher power spectrum [Fig. 5(A)]. Photoinduced bands are observed in the difference spectrum at 592 (not shown), 1067, 1087, 1196, 1412, 1524, and 1632 cm^{-1}. Observation of phototransient bands strongly depends upon excitation wavelength; no Raman bands deriving from transient species were observed with excitation at 240 or 319 nm even with high power, tight focusing conditions.

Figure 6 shows the laser power dependences of the intensities of the 918 cm^{-1} acetonitrile band, the 1196 cm^{-1} photoinduced transient mode, and the 1242 cm^{-1} pyrene fundamental vibration observed with 311 nm excitation. Neutral density filters of varying optical densities were used

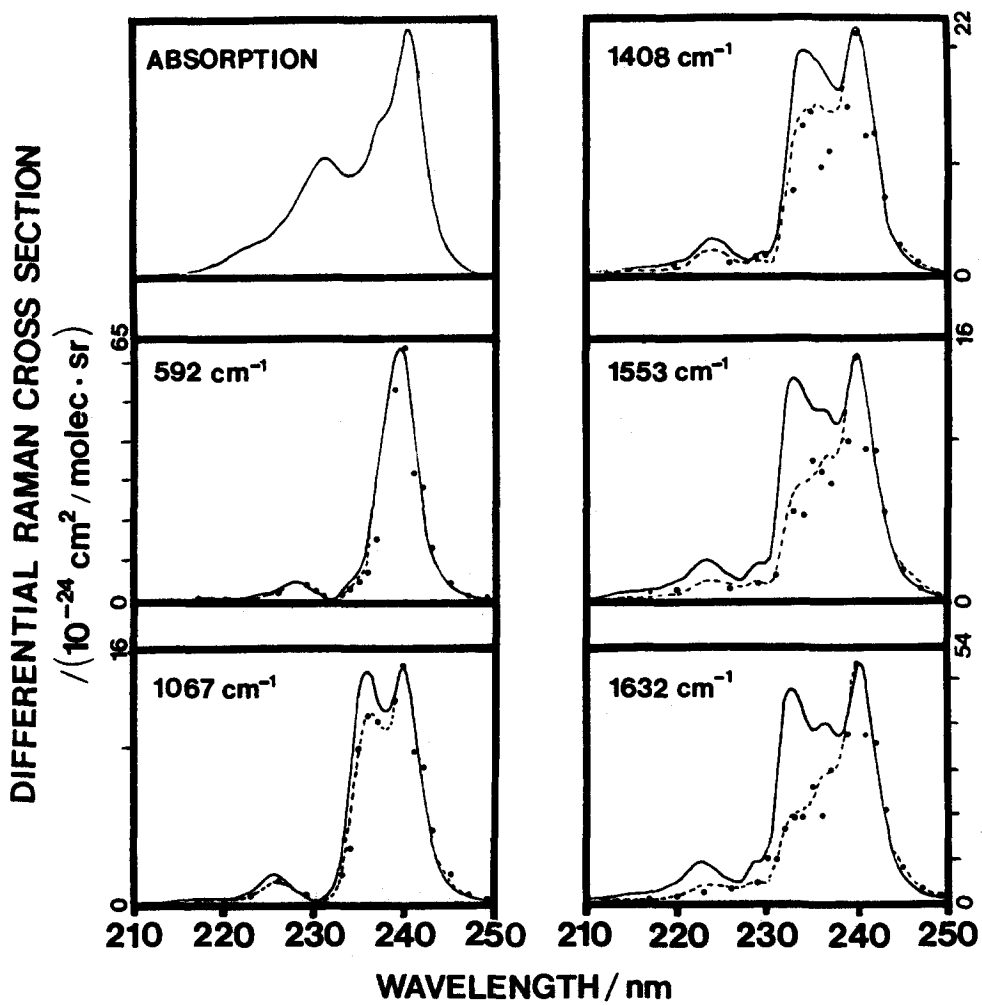

FIG. 4. Resonance Raman excitation profiles of the totally symmetric pyrene fundamental vibrations resonantly enhanced in S_4. Both the experimental profiles (filled circles) and the theoretically predicted curves obtained using basic Condon transform theory (solid lines) and non-Condon transform theory (broken lines) are shown. The theoretical curves are scaled to the experimental data. The S_4 absorption band is also included. The absorption cross section at the absorption maximum (240 nm) is 3.1×10^{-16} cm^2/molecule. The red and blue energy tails of the absorption band have been extrapolated to zero to exclude contributions from the S_3 and S_5 transitions.

Downloaded 22 Jan 2009 to 130.49.228.46. Redistribution subject to AIP license or copyright; see http://jcp.aip.org/jcp/copyright.jsp

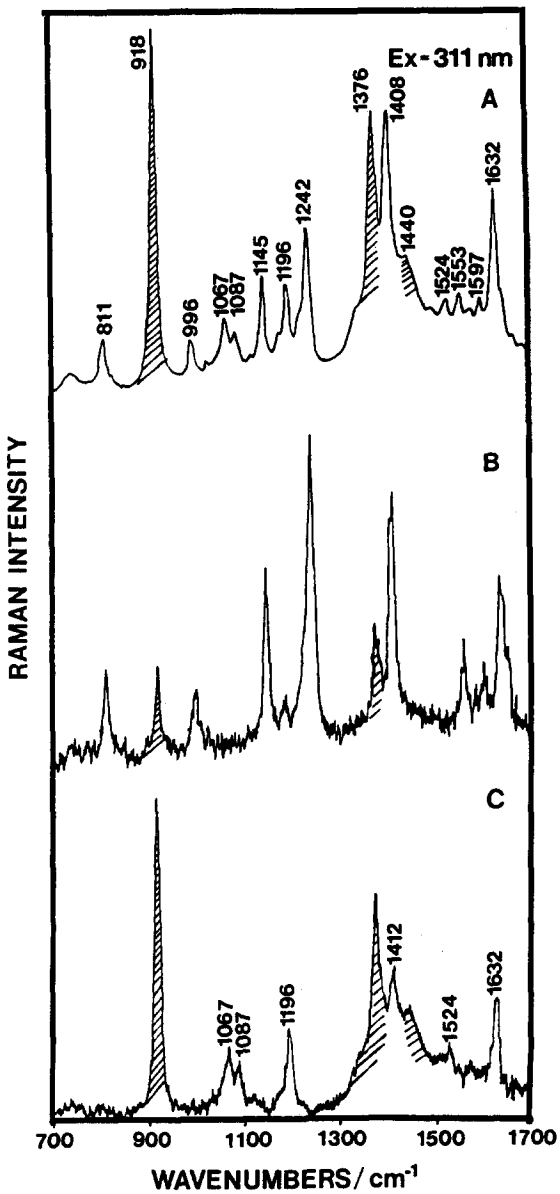

FIG. 5. UV resonance Raman spectra of pyrene excited at 311 nm with incident laser powers of ~10 mW(A) and 0.1 mW(B). The beam is focused to an estimated 500 μm diameter using a 25 cm focal length lens, which leads to estimated energy fluxes of ~250 and 2.5 mJ/cm^2 pulse and power fluxes of ~40 and 0.4 MW/cm^2, respectively. Phototransient Raman bands can be seen in the difference spectrum (C). Acetonitrile bands are shaded.

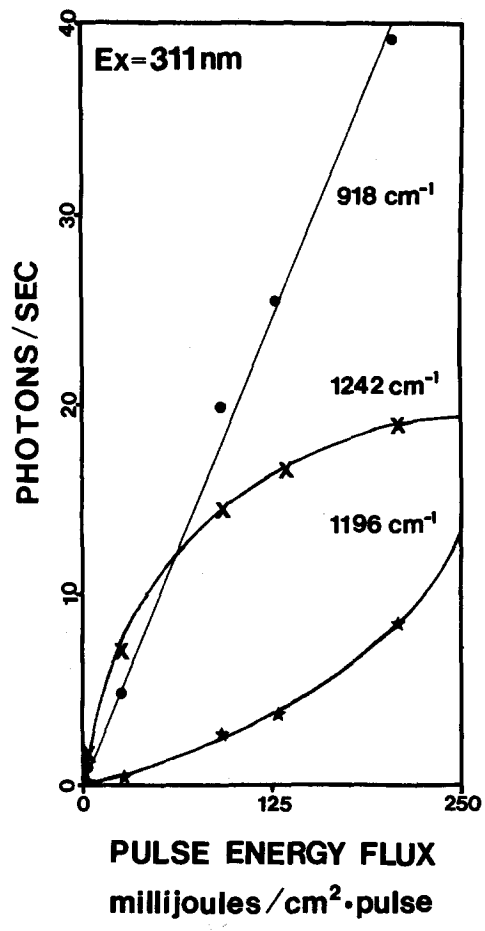

FIG. 6. Laser power dependences of the 918 cm^{-1} acetonitrile band, the 1242 cm^{-1} pyrene fundamental, and the 1196 cm^{-1} phototransient band observed with 311 nm excitation focused to an estimated 500 μm diameter spot size. Pyrene sample concentration was 10^{-3} M. Neutral density filters were used to attenuate the incident laser power.

to attenuate the incident laser power from its maximum average value of 10 mW (~ 250 mJ/cm^2 pulse). As seen in Fig. 6, the 918 cm^{-1} acetonitrile band intensity varies linearly with incident laser power. In contrast, the 1242 cm^{-1} pyrene fundamental intensity increases sublinearly with incident laser power and clearly exhibits saturation at high laser power. The 1196 cm^{-1} phototransient band intensity shows a unique dependence on the incident power; the Raman scattered intensity increases super-linearly with increasing incident laser powers.

DISCUSSION

The absorption spectra of polycyclic aromatic hydrocarbons typically show highly structured UV–visible $\pi \rightarrow \pi^*$ absorption bands which show intense Franck–Condon progressions.[25–28] The high density of vibrational modes along with homogeneous and inhomogeneous band broadening, however, obscure underlying vibronic substructure to give relatively broad, less structured absorption bands.[29] In the case of pyrene, each of the three strong symmetry-allowed $\pi \rightarrow \pi^*$ electronic transitions exhibits distinct Franck–Condon substructure. The different vibronic progressions evident in each electronic transition indicate that different excited state geometric distortions are present in the S_4, S_3, and S_2 electronic transitions.

The $\pi \rightarrow \pi^*$ electronic transitions of conjugated ring systems result in electron density changes which involve primarily the carbon atoms of the rings. Those normal coordinates whose potential energy distributions involve large contributions of in-plane carbon–carbon bond stretching and bending motion will be most strongly enhanced with

Downloaded 22 Jan 2009 to 130.49.228.46. Redistribution subject to AIP license or copyright; see http://jcp.aip.org/jcp/copyright.jsp

excitation in resonance with such transitions. Since the geometric distortion in the excited state occurs along totally symmetric normal coordinates, totally symmetric modes which derive from A-term or Condon sources of Raman scattering are most strongly resonantly enhanced in these transitions.[12,30]

Indeed, our UV resonance Raman spectroscopic investigations of pyrene show strong enhancement of totally symmetric in-plane fundamental ring vibrations. We attempted to correlate the calculated potential energy distributions (PED) of the enhanced vibrations[31] to the electronic transition moments,[19(b)] but were unable to discern any clear pattern that gave qualitative agreement for the S_4, S_3, and S_2 transitions. The highly selective enhancement of particular vibrational modes by each of electronic transitions suggests that unique distortions must occur in each excited state. Our inability to rationalize the enhancement patterns probably is due to the lack of detailed information on the PED along the pyrene internal coordinates; the only existing normal mode calculation groups the internal coordinates. It is also possible, however, that problems exist with the PED calculations[32,33] or the calculated transition dipoles.

Pyrene fundamentals involving carbon–hydrogen vibrations such as the 3024, 3059, and 3103 cm^{-1} modes (see Table I) which are observed in the normal Raman spectra, are not resonantly enhanced with excitation between 220 and 340 nm. The $\pi \rightarrow \pi^*$ transitions should not result in appreciable electron density changes or bond length changes for these vibrations; the coupling of C–H vibrations to $\pi \rightarrow \pi^*$ electronic transitions is expected to be weak.

As expected, both the 592 and 1632 cm^{-1} modes also show strong Raman overtone and combination activity. The strong resonance Raman enhancements for these modes are consistent with the Franck–Condon features observed in the absorption spectrum; vibronic progressions occur $\sim$550 cm^{-1} (237 nm) and 1600 cm^{-1} (231 nm) from the 240 nm absorption maximum.

The enhancement of the 1597 cm^{-1} b_{3g} band derives from a Herzberg–Teller mechanism in which the vibration gains intensity by vibronically coupling the S_4 and S_3 transitions. The role of vibronic coupling in determining the spectroscopic properties of aromatic hydrocarbons, including pyrene, has been extensively discussed in the literature.[34–39] The low oscillator strength S_1 singlet states of PAHs often "borrow" oscillator strength by vibronically coupling with adjacent stronger transitions of the appropriate symmetry. Vibronic coupling activity within the higher excited electronic states of PAHs has also been documented.[37(e)]

Our UVRR study documents vibronic coupling between pyrene's higher excited electronic states. The enhancement of the 1597 cm^{-1} vibration probably derives from a B-term mechanism in which the 1597 cm^{-1} b_{3g} vibration vibronically couples the S_4 and S_3 states. This mode is of the proper symmetry to couple the $S_3(B_{2u})$ and $S_4(B_{1u})$ electronic states. The $S_3(B_{2u})$ and $S_2(B_{1u})$ states can also vibronically couple through b_{3g} modes and an enhancement maximum for this vibration occurs between these electronic transitions. The 280 nm excited spectrum of Fig. 2(b) demonstrates strong enhancement for this vibration with excitation between these transitions.

TRANSFORM THEORY

RREPs for the symmetric vibrational modes enhanced in the S_4 transition were calculated by using the optical transform theory. Transform theory relates the Raman scattering cross sections to the absorption cross section through the use of the optical theorem, the Kramers–Kronig dispersion relation, and recursion relations for harmonic oscillator wave functions. This function is derived in accord with a set of approximations which include (1) the assumption of harmonic vibrational wave functions, (2) linear coupling of the excited electronic potential energy surface with nuclear displacement, and (3) either a full adiabatic approximation in all of the Raman-active modes (i.e., the theory for nonzero temperatures developed by Tonks, Chan, Page, and coworkers[5]) or a full adiabatic approximation in the coordinate of the Raman scattering vibration for which the RREP is being determined (i.e., the theory of Champion, Albrecht, and co-workers[1(a)]). The theoretical development of the transform function has been discussed in detail in the work of Stallard, Champion, Albrecht, Chan, Page, and others.[1,4–6,8]

The transform function for mode m, ϕ_m, evaluated at a particular excitation frequency is

$$\phi_m(\nu) = \frac{1}{\Pi} P \int_0^\infty \frac{\sigma(x)}{x(x-\nu)}\,dx + i\frac{\sigma(\nu)}{\nu}, \tag{3}$$

where P denotes the principal value of the integral. $\sigma(x)$ and $\sigma(\nu)$ are the absorption cross sections (in cm^2/molecule) at frequencies x and ν (in cm^{-1}), respectively, with ν being the excitation frequency. The transform function is related to the resonance Raman scattering polarizability amplitude for mode m as

$$\alpha_m(\nu) \approx |\phi(\nu) - \phi(\nu - \nu_m)|, \tag{4}$$

where ν_m is the vibrational frequency of the Raman mode, m. $\phi(\nu - \nu_m)$ is a function that is blue shifted from the original function $\phi(\nu)$ by the vibrational frequency of the Raman active mode for which the transform is being calculated. The total differential Raman cross section (in cm^2/molecules sr) for a totally symmetric mode using a 90° scattering geometry is proportional to the square of the Raman scattering amplitude and can be expressed as

$$\left(\frac{d\sigma_m(\nu)}{d\Omega}\right)_{\parallel+\perp} = \text{const} \cdot S_m |\phi(\nu) - \phi(\nu - \nu_m)|^2, \tag{5}$$

where the parameter, $S_m = \Delta_m^2/2$ and Δ_m is the displacement of the excited state potential energy surface relative to the ground state along the particular normal coordinate m. The constant contains a ν^4 frequency-dependent term and a Boltzmann term which monitors the occupation of the lowest vibrational level of the Raman-active mode.[8(a)] The constant is also proportional to the square of the solution refractive index n as seen in

$$\text{const} = \tfrac{3}{5}\nu(\nu - \nu_m)^3 n^2 \{[\exp(h\nu_m/kT) - 1]^{-1} + 1\}, \tag{6}$$

where k is the Boltzmann constant and T is the temperature.

The basic transform assumes that non-Condon activity

Downloaded 22 Jan 2009 to 130.49.228.46. Redistribution subject to AIP license or copyright; see http://jcp.aip.org/jcp/copyright.jsp

in the Raman-active mode for which the RREP is being calculated is absent. However, the basic transform expression can be modified to include non-Condon activity in the Raman-active mode by introducing the non-Condon parameter C_m,

$$\left[\frac{d\sigma_m(\nu)}{d\Omega}\right]_{\parallel+\perp}^{nc} = \text{const}\cdot S_m|(1+C_m)\phi(\nu)-(1-C_m)\phi(\nu-\nu_m)|^2, \quad (7)$$

C_m specifies the relative non-Condon activity associated with an excited state displacement along m.[1(a),1(b)]

The experimental and calculated RREP shown in Fig. 4 illustrate that the basic transform theory [Eq. (5)] qualitatively predicts the RREP of only the 592 cm^{-1} mode but fails for higher frequency pyrene fundamental vibrations. The failure of the basic transform is most apparent for the higher frequency modes. The calculated RREPs have high energy features which are much more intense than are experimentally observed. The inclusion of excited state mode frequency changes into the basic transform does not significantly improve the fits. However, the RREPs can be accurately modeled by the addition of a small linear non-Condon coupling contribution.

Table III lists the Franck–Condon coupling strength parameters S_m obtained using the non-Condon transform expression. Also included in the table are the non-Condon parameters C_m utilized to obtain the best fit (by inspection) of the calculated curves to the experimental excitation profiles. S_m is related to Δ_m which is the linear nuclear displacement of the excited state along mode m relative to its root mean square (rms) amplitude in the lowest vibrational level of the ground electronic state. The values for the nuclear displacements Δ_m indicate that for S_4 the potentials are most displaced along the 592 cm^{-1} ($\Delta_m = 1.4$) and 1632 cm^{-1} ($\Delta_m = 0.94$) coordinates. We cannot directly correlate these dimensionless Franck–Condon displacements to changes in particular molecular bond lengths and angles in order to obtain excited state geometry information because of the lack of a detailed PED distribution in the normal mode calculations for pyrene. Table III also includes the product of the non-Condon parameter with the square of the Franck–Condon coupling strength. This product represents the ratio of the vibrationally induced transition moment (due to the mth mode) relative to the allowed transition moment amplitude. The vibrationally induced moment represents only a small fraction of the total moment.

TABLE III. S_4 excited state transform parameters.

Vibrational frequency (cm^{-1})	S_m	Δ_m[a]	C_m	$C_m\sqrt{S_m}$
592	0.46	1.4	0.05	3.4%
1067	0.087	0.59	0.08	2.4%
1408	0.12	0.69	0.1	3.5%
1553	0.07	0.53	0.2	5.3%
1632	0.22	0.94	0.28	13%

[a] $S_m = (\Delta Q_m/2\bar{Q}_m)^2$ where $\bar{Q}_m$ is the rms of the ground state equilibrium position of mode m. Δ_m is $\Delta Q_m/\bar{Q}_m$.

Figure 7 shows that a systematic increase occurs for the non-Condon contributions (the value of C_m) as the vibrational frequency increases. This behavior was predicted by Schomacker *et al.* for systems where nonadiabatic perturbations influence the Raman cross sections.[1(c),40] In systems where both non-Condon and nonadiabatic activity is present, the transform expression for the totally symmetric Stokes fundamental becomes

$$\left(\frac{d\sigma_m(\nu)}{d\Omega}\right)_{\parallel+\perp}^{nc,na} \cong S_m\left|\left(1+C_m+\frac{C_m\nu_m}{\Delta E}\right)\phi(\nu) - \left(1-C_m+\frac{C_m\nu_m}{\Delta E}\right)\phi(\nu-\nu_m)\right|^2, \quad (8)$$

where ΔE is the energy gap between the resonant transition and the electronic state(s) of proper symmetry to nonadiabatically couple through the symmetric mode for which the RREP is being calculated. The symmetric pyrene vibrations can couple the $S_4(B_{1u})$ and $S_2(B_{1u})$ transitions which are separated by an energy gap of $\sim$11 700 cm^{-1}. The data in Fig. 7 show that the observed frequency dependence does not follow the linear dependence predicted by Eq. (8). Each vibrational mode must also show a particular non-Condon contribution which depends upon the degree to which the vibration perturbs the transition moment. A systematic linear dependence upon frequency should occur for nonadiabatic coupling. However, the nonlinear variation of the magnitude C_m with frequency indicates that other parameters also define the magnitude of non-Condon activity.

Preresonant contributions to the Raman intensities from the S_5 (206 nm, B_{3g} or A_g) or S_6 (196 nm, B_{2u}) vacuum UV pyrene transitions did not interfere with our S_4 transform analysis due to their lower oscillator strengths and their large energy separations from S_4.[19] This is confirmed by Table II which shows that the depolarization ratios for the totally symmetric pyrene vibrational modes deviate only slightly from 0.33, the value expected for linearly polarized transitions. Thus, the S_3, S_5, and S_6 transitions negligibly influenced the observed S_4 pyrene cross sections.

Although our present excitation profile measurements within the S_2 and S_3 transitions are compromised by saturation, the relative cross sections of the pyrene bands within each spectrum remains unaffected by saturation, provided that phototransients are not enhanced. Thus, we compared the experimentally observed RREP of the relative intensity ratio between the 592 and 1242 cm^{-1} pyrene bands to that calculated by the Condon transform theory expression [Eq. (5)]. The transform calculation overestimates the relative Raman cross section of the 1242 cm^{-1} band with excitation on the blue side of the S_2 0–0 transition. This behavior is similar to that observed for the high frequency modes in S_4. Thus, we conclude that non-Condon contributions may also be important for enhancement in the S_2 transition.

The use of transform theory to model the S_4 pyrene RREP requires inclusion of a significant non-Condon contribution. This contrasts to the transform modeling of the RREP of the S_1 state of azulene[8(b),8(c)] and the S_1 state of β-carotene,[6] which are accurately modeled within the Condon approximation. The requirement of a non-Condon contribu-

Downloaded 22 Jan 2009 to 130.49.228.46. Redistribution subject to AIP license or copyright; see http://jcp.aip.org/jcp/copyright.jsp

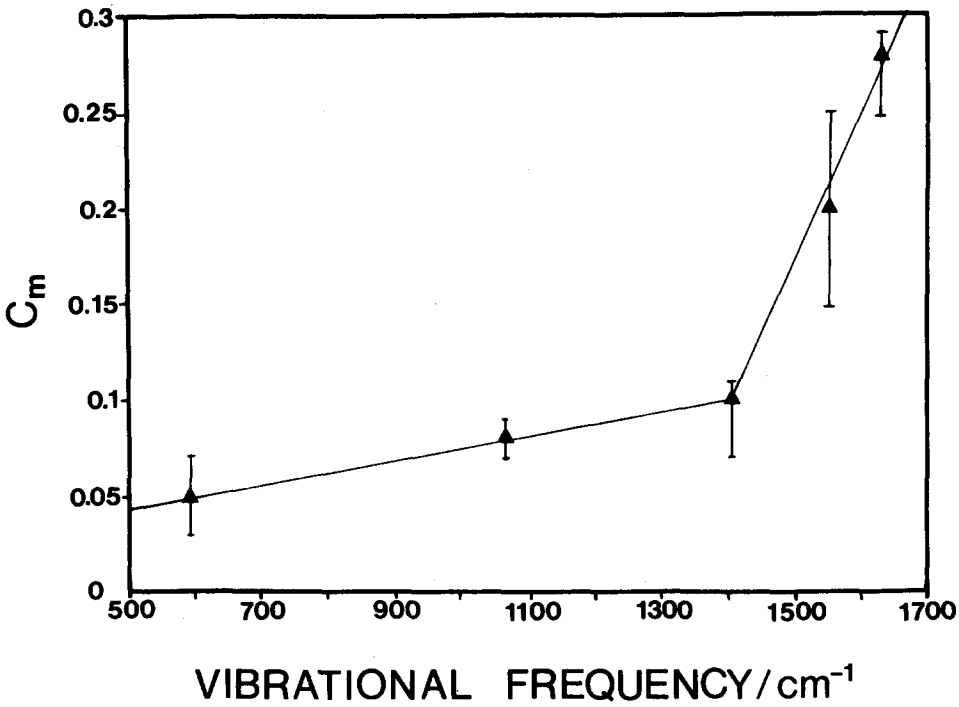

FIG. 7. The vibrational frequency dependence of the non-Condon parameter C_m (see Table III).

tion for modeling of the RREP in the S_4 transition of pyrene is similar to that observed [1(b),1(c)] for ferrocytochrome c excited in the Soret band. Indeed, the relative non-Condon contribution found for the 1362 cm^{-1} mode of ferrocytochrome c is similar to what we find for pyrene.

Our successful transform modeling for the S_4 transition of pyrene stands in sharp contrast to the transform analysis of the S_4 transition of azulene[8(a)] which could only acceptably model the RREP of the 674 cm^{-1} vibration by including excited state frequency changes. Severe disagreement was found between the calculated and observed RREP for all of the other vibrations; incorporation of non-Condon contributions did not significantly improve the fits to the experimental results. Cable and Albrecht concluded that the approximations assumed in the transform theory were invalid for the S_4 azulene excited state. Major excited state structural changes, Duschinsky rotations, vibronic lifetime energy dependences, higher order coupling between electronic states, and interferences from preresonant electronic transitions will compromise the utility of transform theory.

PYRENE RAMAN SATURATION AND STUDIES OF PHOTOCHEMICAL INTERMEDIATES

Saturation of the Raman intensities occurs even with modest incident average laser powers of 2 mW and relatively weak focusing (estimated spot sizes of $\geqslant 500\,\mu$m) because of th high peak pulse energies and peak powers associated with the low duty cycle, ~ 6 ns laser excitation pulse widths; the associated pulse energies and laser power fluxes under such conditions are ~ 0.1 mJ/pulse and 10^7 W/cm^2. Saturation of the pyrene Raman intensities occurs with excitation throughout pyrene's S_2–S_4 electronic transitions and derives from depopulation of ground state pyrene molecules through molecular absorption during excitation within these high oscillator strength transitions. Fast internal conversion processes populate the long-lived ($\geqslant 40$ ns) S_1 excited electronic state.[41] The inherently long lifetime of S_1 bottlenecks relaxation back to the ground energy level. We see no evidence for permanent photochemistry during excitation conditions associated with saturation. Similar saturation phenomena are observed for excitation within the S_2, S_3, and S_4 electronic transitions with similar experimental conditions (molar absorptivity, incident energy flux). Furthermore, fluorescence excitation spectra (not shown) show that the fluorescent quantum yield from S_1 is independent of the electronic absorption band excited (S_2, S_3, or S_4) and simply scales with the molar absorptivity. Thus, the fluorescence data are consistent with a physical picture of Raman saturation deriving from molecular absorption with excitation into these strongly dipole-allowed electronic transitions followed by fast radiationless decay in solution to the bottleneck S_1 electronic state.

The pyrene absorption cross section at the S_4 absorption maximum (240 nm) is 3.1×10^{-16} cm^2/molecule. The differential Raman cross section of the 592 cm^{-1} mode, the vibration most strongly coupled to this electronic transition, is $\sim 64\times 10^{-24}$ cm^2/molecule sr. Thus, the probability of an absorption event is almost a millionfold higher than for Raman.

Figure 8 summarizes the photophysical processes which can occur.[41(a),42] A photon of energy $h\nu_0$ Raman scatters from a ground state pyrene molecule (S_0) to yield a photon of energy $h\nu_R$ (1), or, if absorbed, induces a transition to the resonant S_n excited electronic state (2). Nonradiative decay of S_n results in the population of S_1 (3) which subsequently decays either radiatively by fluorescence (5), or nonradiatively through internal conversion processes (6). At high

Downloaded 22 Jan 2009 to 130.49.228.46. Redistribution subject to AIP license or copyright; see http://jcp.aip.org/jcp/copyright.jsp

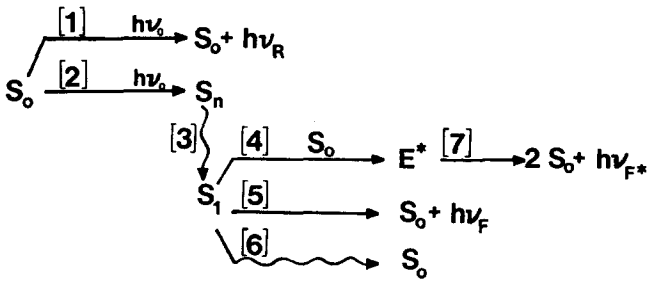

FIG. 8. Photophysical processes involved in pyrene saturation. $h\nu_0$ = incident photon energy, S_0 = ground state pyrene molecule, $h\nu_R$ = Raman scattered photon energy, S_n = upper excited singlet electronic state, S_1 = first excited singlet state, $h\nu_F$ = monomer fluorescence, E^* = excimer, $h\nu_{F^*}$ = excimer fluorescence. Wavy lines designate nonradiative decay processes.

concentrations (10^{-3} M), S_1 can complex with a ground state pyrene molecule S_0 to form an excimer, E^* (4).[42(d),42(e)] The excimer emits (7) a broad blue fluorescence ($h\nu_{f^*}$) that is red shifted from the structured violet monomer fluorescence emission ($h\nu_f$) and dissociates to two ground state pyrene molecules. The 10^{-3} M pyrene samples, indeed, exhibit a blue fluorescence indicating excimer formation. Excimer formation, however, does not contribute to pyrene saturation, since the excimer forms at a diffusion limited rate after population of S_1. Relaxation of the S_1 population is the rate determining step in the pyrene saturation phenomenon.

At high incident energy fluxes new photochemical phenomena occur (see Fig. 5) which, at particular excitation wavelengths, results in the appearance of new Raman bands. The intensities of the transient bands show a super-linear dependence upon incident energy flux. Pyrene photochemical transient Raman bands are observed at 592, 1067, 1087, 1196, 1412, 1524, and 1632 cm^{-1} for 311 nm excitation. The photochemical transient bands do not derive from excited state Raman scattering from S_1 since the frequencies differ significantly from frequencies which have been observed in S_1 low temperature absorption measurements.[24] At high incident energy fluxes, multiphoton ionization can occur to produce pyrene cation radicals. Numerous previous laser photolysis studies of pyrene demonstrated production of cation radicals with excitation within the S_1 and S_2 electronic transitions by a sequential two-photon photoionization process which involves S_1 as an intermediate level.[41(a),42(a),42(b)] We find that S_1 relaxed fluorescence does not continue to increase with increases in incident intensity at excitations where phototransients are formed. This is in contrast to the behavior which occurs when only simple saturation is present and photochemical intermediates do not depopulate S_1. With phototransient formation the relaxed fluorescence intensity reaches a maximum and then decreases as the excitation intensity continues to increase. This decrease apparently signals a depopulation of S_1 associated with photoionization and formation of the pyrene cation.

S_1 becomes populated subsequent to an absorption into the higher pyrene states because of fast relaxation (ps) to S_1. The S_1 excited state lifetime of $\geqslant 40$ ns ensures little relaxation back to the ground state within a single laser excitation pulse. For high incident intensities, and for a significant molar absorptivity for S_1 transitions to higher excited states, an additional photon can be absorbed to ionize and form a radical cation. Provided the radical cation species has a strong absorption band at the laser excitation wavelength, a third photon can resonance Raman scatter from the cation radical species. This obviously requires a high energy flux.

The resonance Raman excitation profiles for photochemically produced radical cation species should be very narrow since

$$I(\nu) \simeq K \cdot \epsilon_g(\nu)\epsilon_{S_1}(\nu)\epsilon^2 R(\nu),$$

where $I(\nu)$ is the observed Raman intensity for the transient at the excitation frequency ν, K is a constant which depends upon the instrumentation, sampling conditions, sample concentration, and Raman cross sections, and $\epsilon(\nu)$ are molar absorptivities, at the excitation frequency where the subscripts g, S_1, and R indicate the ground state, the S_1 excited state, and the cation radical, respectively. Obviously, the probability of observing resonance Raman intensity from the radical cation species is proportional to the probability of absorbing a photon to form S_1 times the probability of S_1 absorbing a photon to form the radical cation. This must be multiplied by the Raman cross section of the radical cation species at the excitation wavelength which is approximately proportional to the square of its molar absorptivity $\epsilon_R^2(\nu)$. Since pyrene is a highly conjugated, polarizable fused macrocycle, similar electronic manifolds are expected for the pyrene molecule and the pyrene radical cation.[43] The major differences in the absorption spectra of these species in the region of the S_1 transition derive from shifts between absorption band maxima. A twofold decrease in the resonance Raman excitation profile bandwidth would be observed for the cation radical compared to that for the ground state species if identical Gaussian absorption bands were present for g, S_1, and R. For a real system, however, shifts occur between absorption bands, and we expect even narrower bandwidths for the "apparent" cation radical excitation profiles. These expectations are consistent with our pyrene photochemical transient studies where photochemical intermediates are observed only over very narrow wavelength intervals.

CONCLUSION

Excitation in resonance with each of the highly structured S_4, S_3, and S_2 excited electronic states of pyrene results in selective, strong enhancement of totally symmetric fundamentals which involve in-plane ring vibrations. The resonance Raman spectra indicate that the 592, 1408, and 1632 cm^{-1} modes most strongly couple to the S_4 electronic transition, whereas different vibrations couple to the S_3 and S_2 transitions. In particular, the 1408 cm^{-1} mode is the most enhanced vibration in S_3 and the 408 and the 1408 cm^{-1} modes are most enhanced in S_2. The Raman cross sections of the 592 and 1632 cm^{-1} modes for 240 nm excitation are ~ 64 and 54 b/sr (1 b = 10^{-24} cm^2/molecule), respectively. By comparison, alkane vibrational Raman cross sections at similar UV excitations are ~ 0.1 mb/sr.[44] The vibrations

Downloaded 22 Jan 2009 to 130.49.228.46. Redistribution subject to AIP license or copyright; see http://jcp.aip.org/jcp/copyright.jsp

most strongly enhanced within the pyrene transitions are those showing Franck–Condon vibronic features in the absorption spectrum. Excitation within the high energy Franck–Condon vibronic features of the S_2–S_4 transitions at 317, 261, and 228 nm results in strong combintion and overtone activity. The 1597 cm^{-1} (b_{3g}) band shows selective enhancement at excitations between the $S_4(B_{1u})$ and $S_3(B_{2u})$ transitions and between the $S_3(B_{2u})$ and $S_2(B_{1u})$ states due to Herzberg–Teller vibronic coupling of these symmetry-allowed electronic transitions.

A comparison between the observed RREP of the totally symmetric pyrene modes in S_4 to those calculated using transform theory show that small non-Condon contributions are required for accurate modeling. The observed frequency dependence of C_m suggests that not only linear, but higher-order electron–nuclear coupling mechanisms contribute to the resonance Raman cross sections.

ACKNOWLEDGMENTS

We would like to thank Dr. C. R. Johnson for helpful discussions and assistance in the early stages of this work. We also wish to thank Professor Paul Champion for a helpful discussion on nonadiabatic contributions in transform theory. We gratefully acknowledge partial support of this work from NIH Grant No. 1R01-GM30741-07. Sanford A. Asher is an Established Investigator of the American Heart Association; this work was done during the tenure of an Established Investigatorship of the American Heart Association and with funds contributed in part by the American Heart Association, Pennsylvania affiliate.

[1](a) B. R. Stallard, P. M. Champion, P. R. Callis, and A. C. Albrecht, J. Chem. Phys. **78**, 712 (1983); (b) B. R. Stallard, P. R. Callis, P. M. Champion, and A. C. Albrecht, *ibid.* **80**, 70 (1984); (c) K. T. Schomacker, O. Bangcharoenpaurpong, and P. M. Champion, *ibid.* **80**, 4701 (1984); (d) P. M. Champion and A. C. Albrecht, Annu. Rev. Phys. Chem. **33**, 353 (1982); Chem. Phys. Lett. **82**, 410 (1981).

[2](a) S. Y. Lee, E. J. Heller, J. Chem. Phys. **71**, 4777 (1979); (b) E. J. Heller, R. L. Sundberg, and D. Tannor, J. Phys. Chem. **86**, 1822 (1982); (c) D. J. Tannor and E. J. Heller, J. Chem. Phys. **77**, 202 (1982).

[3]V. Hizhnyakov and I. Tehver, Phys. Status Solidi **21**, 755 (1967).

[4]D. C. Blazej and W. L. Peticolas, J. Chem. Phys. **72**, 3134 (1980).

[5]D. L. Tonks and J. B. Page, Chem. Phys. Lett. **66**, 449 (1979).

[6]C. K. Chan and J. B. Page, J. Chem. Phys. **79**, 5234 (1983).

[7]A. B. Myers, R. A. Harris, and R. A. Mathies, J. Chem. Phys. **79**, 603 (1983).

[8](a) J. R. Cable and A. C. Albrecht, J. Chem. Phys. **84**, 1969 (1986); (b) O. Brafman, C. K. Chan, B. Khodadoost, J. B. Page, and C. T. Walker, *ibid.* **80**, 5406 (1984); (c) C. K. Chan, J. B. Page, O. Brafman, B. Khodadoost, and C. T. Walker, *ibid.* **82**, 4813 (1985).

[9](a) S. A. Asher and C. R. Johnson, Science **225**, 311 (1984); (b) C. R. Johnson and S. A. Asher, Anal. Chem. **56**, 2261 (1984); (c) S. A. Asher and C. M. Jones, Am. Chem. Soc. Fuel Sci. **31**, 170 (1986).

[10]C. M. Jones, T. A. Naim, M. Ludwig, J. Murtaugh, P. L. Flaugh, J. M. Dudik, C. R. Johnson, and S. A. Asher, Trends Anal. Chem. **4**, 75 (1985).

[11]R. Rumelfanger, S. A. Asher, and M. B. Perry, Appl. Spectrosc. **42**, 267 (1988).

[12]A. Y. Hirakawa and M. Tsuboi, in *Vibrational Spectra and Structure*, edited by J. R. Durig (Elsevier, New York, 1983), p. 145, Vol. 12.

[13]C. M. Jones, V. L. DeVito, P. A. Harmon, and S. A. Asher, Appl. Spectrosc. **41**, 1268 (1987).

[14]S. A. Asher, C. R. Johnson, and J. Murtaugh, Rev. Sci. Instrum. **54**, 1657 (1983).

[15]C. R. Johnson, M. Ludwig, and S. A. Asher, J. Am. Chem. Soc. **108**, 905 (1986).

[16]M. Ludwig and S. A. Asher, J. Am. Chem. Soc. **110**, 1005 (1988).

[17]J. M. Dudik, C. R. Johnson, and S. A. Asher, J. Chem. Phys. **82**, 1732 (1985).

[18]R. S. Mulliken, J. Chem. Phys. **23**, 1997 (1955).

[19](a) R. S. Becker, I. S. Singh, and E. A. Jackson, J. Chem. Phys. **38**, 2144 (1963); (b) R. L. Hummel and K. Ruedenberg, J. Phys. Chem. **66**, 2334 (1962).

[20]P. A. Geldof, R. P. H. Rettschnick, and G. J. Hoytink, Chem. Phys. Lett. **10**, 549 (1971).

[21]A. Bree, R. A. Kydd, T. N. Misra, and V. V. B. Vilkos, Spectrochim. Acta Part A **27**, 2315 (1971).

[22]R. Mecke and W. E. Klee, Z. Elektrochem. **65**, 327 (1961).

[23]J. Ferguson, L. W. Reeves, and W. G. Schneider, Can. J. Chem. **35**, 1117 (1957).

[24]L. A. Klimova, Opt. Spectrosc. **15**, 185 (1963).

[25]E. Heilbronner and H. Bock, *The HMO Model and Its Application* (Wiley–Interscience, New York, 1976).

[26]R. A. Friedel and M. Orchin, *Ultraviolet Spectra of Aromatic Compounds* (Wiley, New York, 1951).

[27]H. H. Jaffe and M. Orchin, *Theory and Applications of Ultraviolet Spectroscopy* (Wiley, New York, 1962).

[28]E. F. McCoy and I. G. Ross, Aus. J. Chem. **15**, 573 (1962).

[29]P. M. Champion and A. C. Albrecht, J. Chem. Phys. **72**, 6498 (1980).

[30]D. P. Craig, J. Chem. Soc. **1950**, 2146.

[31]N. Neto and C. DiLauro, Spectrochim. Acta Part A **26**, 1175 (1970).

[32]H. Matsura and M. Tasumi, in *Vibrational Spectra and Structure*, edited by J. R. Durig (Elsevier, New York, 1983), p. 69, Vol. 12.

[33]G. Fogarasi and P. Pulay, in *Vibrational Spectra and Structure*, edited by J. R. Durig (Elsevier, New York, 1985), p. 125, Vol. 14.

[34]G. Orlandi and W. Siebrand, J. Chem. Phys. **58**, 4513 (1973).

[35]G. Herzberg and E. Teller, Z. Phys. Chem. B **21**, 410 (1933).

[36]J. Tang and A. C. Albrecht, in *Raman Spectroscopy, Theory and Practice*, edited by H. A. Syzmanski (Plenum, New York, 1970), Vol. II.

[37](a) R. M. Hochstrasser, Acc. Chem. Res. **1**, 266 (1968); (b) F. M. Garfirth, C. K. Ingold, and H. G. Poole, J. Chem. Soc. **1948**, 406; (c) D. S. McClure, J. Chem. Phys. **22**, 1668 (1954); (d) D. P. Craig, J. M. Hollas, M. F. Redies, and S. C. Wait, Jr., Proc. Chem. Soc. **1959**, 361.

[38]N. Kanamaru and E. C. Lim, Chem. Phys. Lett. **35**, 303 (1975).

[39]K. Cunningham, W. Siebrand, and D. F. Williams, Chem. Phys. Lett. **20**, 496 (1973).

[40]G. J. Small and E. S. Yeung, Chem. Phys. **9**, 379 (1975).

[41](a) G. E. Hall and G. A. Kenney-Wallace, Chem. Phys. **28**, 205 (1978); (b) P. Seybold and M. Gouterman, Chem. Rev. **55**, 413 (1965).

[42](a) J. T. Richards, G. West, and J. K. Thomas, J. Phys. Chem. **74**, 4137 (1970); (b) M. Ottolenghi, Chem. Phys. Lett. **2**, 339 (1971); (c) A. R. Watkins, J. Phys. Chem. **80**, 713 (1976); (d) V. Forster and K. Kasper, Z. Elektrochem. **59**, 976 (1955); (e) C. H. J. Wells, *Introduction to Molecular Photochemistry* (Chapman and Hall, London, 1972).

[43]G. E. Hall and G. A. Kenney-Wallace, Chem. Phys. **32**, 313 (1978).

[44]M. O. Trulson and R. A. Mathies, J. Chem. Phys. **84**, 2068 (1986).

Downloaded 22 Jan 2009 to 130.49.228.46. Redistribution subject to AIP license or copyright; see http://jcp.aip.org/jcp/copyright.jsp